

## Subdivision of the Bacterioferritin Comigratory Protein Family of Bacterial Peroxiredoxins Based on Catalytic Activity<sup>†</sup>

David J. Clarke,<sup>‡</sup> Ximena P. Ortega,<sup>§</sup> C. Logan Mackay,<sup>‡</sup> Miguel A. Valvano,<sup>§</sup> John R. W. Govan,<sup>||</sup>  
Dominic J. Campopiano,<sup>‡</sup> Pat Langridge-Smith,<sup>‡</sup> and Alan R. Brown<sup>\*,||,⊥</sup>

<sup>‡</sup>SIRCAMs, School of Chemistry, University of Edinburgh, Edinburgh, U.K., <sup>§</sup>Infectious Diseases Research Group, Department of Microbiology and Immunology, University of Western Ontario, Ontario, Canada, and <sup>||</sup>Centre for Infectious Diseases, University of Edinburgh, Edinburgh, U.K. <sup>⊥</sup>Current address: School of Biosciences, Geoffrey Pope Building, University of Exeter, Stocker Road, Exeter EX4 4QD, U.K.

Received October 1, 2009; Revised Manuscript Received January 14, 2010

**ABSTRACT:** Peroxiredoxins are ubiquitous proteins that catalyze the reduction of hydroperoxides, thus conferring resistance to oxidative stress. Using high-resolution mass spectrometry, we recently reclassified one such peroxiredoxin, bacterioferritin comigratory protein (BCP) of *Escherichia coli*, as an atypical 2-Cys peroxiredoxin that functions through the formation of an intramolecular disulfide bond between the active and resolving cysteine. An engineered *E. coli* BCP, which lacked the resolving cysteine, retained enzyme activity through a novel catalytic pathway. Unlike the active cysteine, the resolving cysteine of BCP peroxiredoxins is not conserved across all members of the family. To clarify the catalytic mechanism of native BCP enzymes that lack the resolving cysteine, we have investigated the BCP homologue of *Burkholderia cenocepacia*. We demonstrate that the *B. cenocepacia* BCP (*BcBCP*) homologue functions through a 1-Cys catalytic pathway. During catalysis, *BcBCP* can utilize thioredoxin as a reductant for the sulfenic acid intermediate. However, significantly higher peroxidase activity is observed utilizing glutathione as a resolving cysteine and glutaredoxin as a redox partner. Introduction of a resolving cysteine into *BcBCP* changes the activity from a 1-Cys pathway to an atypical 2-Cys pathway, analogous to the *E. coli* enzyme. In contrast to the native *B. cenocepacia* enzyme, thioredoxin is the preferred redox partner for this atypical 2-Cys variant. BCP-deficient *B. cenocepacia* exhibit a growth-phase-dependent hypersensitivity to oxidative killing. On the basis of sequence alignments, we believe that *BcBCP* described herein is representative of the major class of bacterial BCP peroxiredoxins. To our knowledge, this is the first detailed characterization of their catalytic activity. These studies support the subdivision of the BCP family of peroxiredoxins into two classes based on their catalytic activity.

Reactive oxygen species (ROS)<sup>1</sup> arising from the incomplete reduction of oxygen are an inevitable consequence of aerobic metabolism and result in wide-ranging oxidative damage to nucleic acids, proteins, and lipids. Organisms occupying aerobic environments have evolved numerous reductive defense mechanisms against ROS. Peroxiredoxins (Prxs), which undertake the thiol-dependent reduction of peroxide substrates, constitute one such defense mechanism. The catalytic activity of Prxs can be divided into 1-Cys and 2-Cys pathways based on the number of cysteines required for catalysis. The 2-Cys Prxs are further

divided into typical and atypical 2-Cys peroxidases; typical 2-Cys Prxs being obligate dimers, while atypical 2-Cys Prxs are monomeric. During the reduction of hydroperoxides, all Prxs share a common first step, which involves an active (peroxidatic) cysteine thiolate attacking the peroxide substrate, resulting in the formation of a sulfenic acid (Cys-SOH) intermediate on the active cysteine. Thereafter, different pathways may be employed in the resolution of the sulfenic acid intermediate, and it is variation in this process which leads to the delineation of the Prxs into 1-Cys and 2-Cys peroxidases (1). 2-Cys Prxs contain a second cysteine, termed the resolving cysteine, which attacks the sulfenic acid intermediate of the active cysteine, forming a disulfide bond that is subsequently reduced by a cell-specific oxidoreductase. The disulfide bond between the active and resolving cysteine can be either intramolecular (monomeric atypical 2-Cys pathway) or intermolecular (dimeric typical 2-Cys). In contrast, 1-Cys Prxs do not harbor a resolving cysteine. In this case, the sulfenic acid intermediate is thought to be resolved by thiol-containing reductants such as glutathione or thioredoxin.

The bacterioferritin comigratory protein (BCP) family of Prxs was first characterized in *Escherichia coli* (2). BCP is a monomeric protein with thiol-dependent peroxidase activity, which until recently was assumed to function via a 1-Cys mechanism, based on observations made of the *E. coli* enzyme. However, by applying high-resolution mass spectrometry, we recently reclassified *E. coli* BCP (*EcBCP*) as an atypical 2-Cys enzyme,

<sup>†</sup>This work was undertaken under the framework of the U.K. Cystic Fibrosis Microbiology Consortium, an initiative funded by the Big Lottery Fund in association with the Cystic Fibrosis Trust. Additional support was provided by the RASOR consortium, EPSRC, BBSRC, and the University of Edinburgh, and the Canadian Cystic Fibrosis Foundation (to M.A.V.). M.A.V. holds a Canada Research Chair in Infectious Diseases and Microbial Pathogenesis.

\*Corresponding author. Tel: +44-(0)1392-725526. Fax: +44-(0)1392-263434. E-mail: a.r.brown@exeter.ac.uk.

Abbreviations: BCP, bacterioferritin comigratory protein; *EcBCP*, BCP of *Escherichia coli*; *BcBCP*, BCP of *Burkholderia cenocepacia*; *XcBCP*, BCP of *Xanthomonas campestris*; Prx, peroxiredoxin; ROS, reactive oxygen species; CF, cystic fibrosis; Bcc, *Burkholderia cepacia* complex; WT, wild type; Trx, thioredoxin; TrxR, thioredoxin reductase; GSH, reduced glutathione; Grx, glutaredoxin; IAM, iodoacetamide; NEM, N-ethylmaleimide; TCEP, tris(2-carboxyethyl)phosphine hydrochloride; FT-ICR-MS, Fourier transform ion cyclotron resonance mass spectrometry; MS, mass spectrometry; ECD, electron capture dissociation; CID, collision-induced dissociation.

Table 1: Strains and Plasmids<sup>a</sup>

strain or plasmid	relevant characteristics	source and/or ref
<i>B. cenocepacia</i> strains		
K56-2	ET12 clone related to genome sequence strain, J2315; CF clinical isolate	BCCM; 33
XOA14	K56-2, <i>bcp::pGPΩTp</i> , <i>Tp<sup>r</sup></i>	7
ARB201	XOA14, pARB10 (encoding a functional <i>BcBCP</i> protein), <i>Tp<sup>r</sup></i> , <i>Tet<sup>r</sup></i>	this study
<i>E. coli</i> strains		
DH5α	F <sup>−</sup> F80d <i>lacZ</i> Δ <i>M15</i> Δ( <i>lacZYA-argF</i> )U169 <i>recA1</i> <i>endA1 hsdR17</i> (r <sub>k</sub> <sup>−</sup> , m <sub>k</sub> <sup>+</sup> ) <i>phoA supE44 λ<sup>−</sup> thi-1 gyrA96 relA1</i>	Invitrogen
BL21(DE3)	F <sup>−</sup> <i>ompT hsdS<sub>B</sub></i> (r <sub>B</sub> <sup>−</sup> m <sub>B</sub> <sup>−</sup> ) <i>gal dcm</i> (DE3)	Novagen
plasmids		
pET-28a	<i>ori<sub>pBR322</sub></i> , Kan <sup>r</sup> , <i>P<sub>T7lac</sub></i>	Novagen
pDA17	<i>ori<sub>pBBR1</sub></i> , Tet <sup>r</sup> , <i>mob<sup>+</sup></i> , <i>P<sub>dhfr</sub></i>	D. Aubert
pARB1	pET28a encoding WT <i>BcBCP</i>	this study
pARB2	pET28a encoding C44S <i>BcBCP</i>	this study
pARB3	pET28a encoding C98S <i>BcBCP</i>	this study
pARB4	pET28a encoding L49C <i>BcBCP</i>	this study
pARB5	pET28a encoding WT <i>EcBCP</i>	3
pARB10	pDA17 encoding WT <i>BcBCP</i>	this study

<sup>a</sup>Abbreviations: *Tp<sup>r</sup>*, trimethoprim resistance; *Tet<sup>r</sup>*, tetracycline resistance; Kan<sup>r</sup>, kanamycin resistance; BCCM, Belgian Coordinated Collection of Micro-organisms.

functioning via the formation of an intramolecular disulfide bond between an active and resolving cysteine (3). Sequence alignments of prokaryotic BCP homologues revealed that the majority of homologues lack the resolving cysteine and as such would be expected to function via a 1-Cys catalytic process. However, an engineered *EcBCP*, in which the resolving cysteine was replaced with a serine (C50S), retained peroxidatic activity through a novel catalytic mechanism distinct from the anticipated 1-Cys pathway (3).

BCP homologues lacking a resolving cysteine have been assumed to function via the 1-Cys Prx pathway. However, the mechanistic details of such enzymes have never been fully characterized. In light of the novel pathway adopted by the engineered *EcBCP* C50S enzyme (3), we sought to define the catalytic mechanism employed by native BCP homologues that lack a resolving cysteine. We herein characterize one such member of the BCP family: the BCP Prx of *Burkholderia cenocepacia*, an aerobic Gram-negative organism that belongs to a group of closely related bacterial species referred to as the *Burkholderia cepacia* complex (Bcc) (4). *B. cenocepacia* is a significant pathogen of the cystic fibrosis (CF) lung, an environment that is considered highly oxidative as a consequence of the profound influx of neutrophils and the resulting release of ROS. In addition, *B. cenocepacia* is capable of surviving the oxidative burst within activated macrophages (5, 6). Consequently, antioxidant activities are thought to play a role in the ability of this organism to establish chronic infection of the CF airways.

We previously reported that the *bcp* homologue of *B. cenocepacia* is coexpressed with the *arn* locus (7). The *arn* locus encodes the biosynthetic enzymes required for the modification of lipopolysaccharide with aminoarabinose, a positively charged sugar that lowers the binding affinity of cationic antimicrobial peptides, thus conferring resistance (8). Such antimicrobial peptides are the dominant mechanism of nonoxidative killing by phagocytic cells. Thus, the genetic linkage of *bcp* with the *arn* locus within *Burkholderia* species combines putative resistance mechanisms against both oxidative and nonoxidative killing by phagocytes. In the present study, we demonstrate that the BCP of *B. cenocepacia* displays the anticipated thiol-dependent peroxidase activity, which protects against oxidative stress in a growth-phase-dependent manner. The native enzyme, which lacks a resolving

cysteine, functions via a 1-Cys catalytic pathway, while introduction of a resolving cysteine switches the catalytic pathway to an atypical 2-Cys mechanism that is functionally indistinguishable from that of the *E. coli* enzyme. We conclude that the BCP family of bacterial Prxs can be subdivided on the basis of catalytic activity and that the 1-Cys peroxidatic mechanism, typified by the *Burkholderia* enzyme, represents the dominant class.

## EXPERIMENTAL PROCEDURES

**Bacterial Strains, Macrophages, and Culture Conditions.** *B. cenocepacia* strain K56-2 was used in this study. Based on multilocus sequence typing (MLST), *B. cenocepacia* K56-2 belongs to the same clonal complex as the genome sequence strain *B. cenocepacia* J2315, a representative of the highly transmissible ET12 epidemic lineage. *B. cenocepacia* XOA14 was created by insertional inactivation of the *B. cenocepacia* K56-2 *bcp* homologue (corresponding to BCAL1936 of *B. cenocepacia* J2315) using the pGPΩTp suicide plasmid (9). *E. coli* strains DH5α and BL21(DE3) were used for cloning and protein expression, respectively. All bacterial strains were routinely grown at 37 °C in Luria–Bertani (LB) medium. *Burkholderia* cultures were supplemented as required with 100 μg/mL trimethoprim (Tp), 100 μg/mL tetracycline (Tet), and/or 50 μg/mL gentamicin (Gm). *E. coli* cultures were supplemented with Tp (50 μg/mL), Tet (20 μg/mL), or kanamycin (30 μg/mL). Bacterial strains are listed in Table 1.

The murine macrophage cell line RAW264.7 was obtained from the American Type Culture Collection. ANA1 macrophages were a gift of Danuta Radzioch, McGill University, Quebec, Canada. Cells were maintained in DMEM with 10% fetal bovine serum and grown at 37 °C with 5% carbon dioxide.

**Cloning and Site-Directed Mutagenesis of BCP.** The *bcp* gene of *B. cenocepacia* K56-2 was PCR amplified (PfuUltra II fusion HS DNA polymerase; Stratagene), incorporating *NdeI* and *BamHI* restriction sites into the forward and reverse primers, respectively, enabling ligation into *NdeI*/*BamHI*-digested pET-28a vector (Novagen). This resulting vector, pARB1, encodes wild-type (WT) *BcBCP* with an N-terminal 6-His tag. His-tagged WT *EcBCP* was expressed from a comparable vector (pARB5) following amplification of the open reading frame

from *E. coli* K12. Using pARB1 vector as template and the QuikChange II site-directed mutagenesis kit (Stratagene), three mutant open reading frames of BcBCP were created: C44S (pARB2), C98S (pARB3), and L49C (pARB4). The resulting plasmids (pARB1–pARB5) were used to transform *E. coli* strain BL21(DE3). Primer sequences used for cloning and site-directed mutagenesis are available upon request.

**Expression and Purification of BCP Enzymes.** *E. coli* BL21(DE3) cells transformed with the appropriate BCP-encoding plasmid were cultured overnight at 37 °C in 50 mL of LB medium supplemented with kanamycin (30 µg/mL). Overnight cultures were used to inoculate 1 L of fresh medium, which was cultured to an optical density at 600 nm of approximately 0.6. Isopropyl 1-thio-β-D-galactopyranoside (IPTG) was added to a final concentration of 0.25 mM, and cultures were incubated for 3 h. Cells were harvested by centrifugation and resuspended in 20 mL of Tris (50 mM), NaCl (500 mM), and imidazole (20 mM), pH 7.5. Cells were disrupted by sonication and lysates centrifuged. Clarified supernatant was filtered (0.45 µm) prior to loading onto a HisTrap FF 5 mL column (GE Healthcare). His-tagged BCP protein was eluted from the nickel column with increasing imidazole concentration and desalted using a PD Miditrap G-25 column (GE Healthcare), eluting in Hepes–NaOH (pH 7.0).

**Determination of Thioredoxin-Linked Peroxidase Activity of BCP.** Thioredoxin-linked peroxidase activity was assessed essentially as described previously (2). In brief, reactions were performed at room temperature in 500 µL volumes, comprising 0.36 µM thioredoxin reductase (TrxR; Sigma-Aldrich), 1.7 µM thioredoxin (Trx; Sigma Aldrich), 0.1 mM hydrogen peroxide, and 0.2 mM NADPH (Roche) in 50 mM Hepes–NaOH (pH 7). BCP concentrations were variable, ranging from 0 to 16 µM. Peroxide was added to the reaction mixture last, and the absorbance at 340 nm was measured continuously for 5 min. The assay was also performed with 1 mM GSH in the reaction mixture.

**Determination of Glutaredoxin-Linked Peroxidase Activity of BCP.** Reactions were performed at room temperature in 500 µL volumes, comprising 1 unit of glutathione reductase (Calbiochem), 12 µM glutaredoxin (Grx; Calbiochem), 1 mM reduced glutathione (GSH; Sigma-Aldrich), 0.1 mM hydrogen peroxide, and 0.15 mM NADPH (Roche) in 50 mM Hepes–NaOH (pH 7). BCP concentrations were variable, ranging from 0 to 16 µM. Peroxide was added to the reaction mixture last, and the absorbance at 340 nm was measured continuously for 5 min.

**H<sub>2</sub>O<sub>2</sub> Oxidation.** Typically, wild-type and mutant BCP proteins were at a concentration of 50 µM in ammonium acetate (100 mM, pH 7.2); GSH was added to a final concentration of 1 mM before reaction with H<sub>2</sub>O<sub>2</sub>. Typically, oxidation was allowed to proceed for a few seconds before the addition of 4-fold H<sub>2</sub>O–MeOH–HCOOH (50:48:2 v/v/v) quenched the reaction.

**Preparation of Reduced Thioredoxin and Glutaredoxin.** Thioredoxin and glutaredoxin were resuspended in 100 mM ammonium acetate (pH 7.2) before reduction with 2 mM TCEP. Excess TCEP was removed by buffer exchange using a PD-Miditrap desalting column (GE Healthcare), and the sample was eluted in 50 mM ammonium acetate, pH 5.5. Disulfide bond reduction was verified by FT-ICR-MS, and the reduced protein was stored at 4 °C. Protein concentration was measured using the BCA assay (Pierce, Rockford, IL).

**Reaction of Oxidized BCP Species with Reduced Thioredoxin or Glutaredoxin.** Oxidized wild-type and L49C BCP species were produced by treatment of 50 µM protein with 100 µM hydrogen peroxide, in the presence of 1 mM GSH. The resulting oxidized species were purified by a PD-Miditrap desalting column (GE Healthcare) and eluted with 200 mM ammonium acetate (pH 7.2). The samples (10 µM) were then treated with 10 µM reduced thioredoxin or glutaredoxin and incubated at room temperature for 5 min. The reaction was quenched with 2-fold H<sub>2</sub>O–MeOH–HCOOH (50:48:2 v/v/v) and analyzed by FT-ICR-MS.

**FT-ICR Mass Spectrometry.** Protein samples were buffer exchanged into 100 mM ammonium acetate, pH 7.4, before addition of hydrogen peroxide and mass spectrometry analysis. Reactions were quenched with 2-fold H<sub>2</sub>O–MeOH–HCOOH (50:48:2 v/v/v) and analyzed by FT-ICR-MS. Mass spectrometry data were acquired on an Apex Ultra Qh-FT-ICR mass spectrometer equipped with a 12 T superconducting magnet and an electrospray ion source (Bruker Daltonics, Billerica, MA). Nano-ESI was performed using a TriVersa Nanomate (Advion Bio-Sciences, Ithaca, NY) running in infusion mode. Broad-band data were typically acquired between *m/z* 600 and 4000 for 0.5 s, and each spectrum was the sum of 32 scans. The mass spectra were externally calibrated using ES tuning mix (Agilent) and analyzed using DataAnalysis software (Bruker Daltonics). Isotope distributions of specific charge states were predicted using IsotopePattern software (Bruker Daltonics) from theoretical empirical formulas. These were overlaid upon the recorded experimental data as scatter plots, with the theoretical apex of each isotope peak designated by a circle.

**Top-Down FT-ICR-Tandem Mass Spectrometry.** Top-down fragmentation was performed on the 12T Qh-FT-ICR. First, a specific ion species was isolated with the instrument's mass resolving quadrupole, and MS/MS was performed using collision-induced dissociation (CID) or electron capture dissociation (ECD). For CID, the collision voltage was typically set between 20 and 35 V. For ECD, 1.8 A was applied to the dispenser cathode filament (Heatwave Technologies) and 20 V to the lens, and a pulse of 4–9 ms was employed. Fragmentation data were the sum of 250–750 scans, and data analyses were performed using DataAnalysis (Bruker Daltonics). The SNAP algorithm was used for automated peak picking, and the resulting top-down fragment mass lists were searched against the primary sequence of BCP using Prosight-PTM software (10, 11). Mass error tolerances were set for all Prosight searches at 10 ppm.

**Complementation of BCP Function.** The N-terminal 6-His-tagged WT *bcp* ORF was PCR amplified from pARB1, incorporating *EcoRI* and *XbaI* restriction sites into the forward and reverse primers, respectively. The ORF was subsequently ligated into *EcoRI*- and *XbaI*-digested pDA17 vector (Tet<sup>R</sup>), generating pARB10. pARB10 was introduced into XOA14 by triparental mating, resulting in strain ARB201. Expression of 6-His-tagged BcBCP was confirmed by Western analysis of whole-cell lysates using anti-His antibody (GE Healthcare) and HRP-linked anti-mouse IgG (Cell Signaling Technology).

**Expression Analysis of BCP.** *B. cenocepacia* K56-2 was grown to logarithmic phase in LB prior to isolation of RNA (RNeasy protect bacteria mini; Qiagen), DNase treatment (RNase-free DNase set; Qiagen), and subsequent cDNA synthesis (SuperScript III reverse transcriptase; Invitrogen). To assess expression of *bcp* and representative genes from the upstream *arn* locus (*arnT* and *arnB*), quantitative real-time PCR (QRT-PCR)



was performed using the platinum SYBR green qPCR supermix-UDG (Invitrogen) in a 25  $\mu$ L reaction volume containing 10  $\mu$ L of 1 in 100 diluted cDNA, 400 nM primers, and 4% (v/v) DMSO. All primer pairs exhibited PCR efficiencies between 90% and 104%, with  $R^2$  values greater than 0.99 over at least a  $10^3$  range of template concentrations. Primer sequences are available upon request. Thermal cycling was performed on a Stratagene Mx3000P thermal cycler, and data were analyzed using the comparative quantitation algorithm. Dissociation curve analysis and electrophoresis of representative samples confirmed the identity of PCR products.

Northern blot analysis was performed according to standard procedures, with  $^{32}$ P-labeled probes prepared using the Rad-Prime DNA labeling system (Invitrogen).

**Assessment of Sensitivity to Hydrogen Peroxide.** Strains were grown in LB without supplements. At appropriate time points throughout the growth phase, culture aliquots were removed to fresh culture vessels and challenged with either hydrogen peroxide (to a final concentration of 1 mM) or an equivalent volume of PBS (control). After 30 min incubation at 37 °C, appropriate serial dilutions were plated, allowing viable counts and percentage survival to be determined.

**Macrophage Infection Assays.** Macrophage infection assays were performed to assess intracellular survival of *B. cenocepacia*. To quantify intracellular survival, bacteria were added to macrophages at a multiplicity of infection (MOI) of 50 bacteria per macrophage, and internalization of bacteria was allowed to proceed for 2 h. Following internalization, cell culture medium was supplemented with ceftazidime (1 mg/mL) and kanamycin (500  $\mu$ g/mL) to kill remaining extracellular bacteria. The number of surviving intracellular bacteria at 2 and 4 h postinternalization was determined by triplicate plating of serially diluted macrophage cell lysate.

Localization of *Burkholderia* within macrophages was assessed using tetramethylrhodamine-dextran (TMR-dextran) to label lysosomes and LysoTracker Red to label acidic compartments. For lysosome labeling prior to bacterial infection, ANA-1 macrophages were incubated with 250  $\mu$ g/mL TMR-dextran (Molecular Probes) for 2 h, followed by a 1 h chase in dye-free medium to ensure full delivery of TMR-dextran to lysosomes. Macrophages were infected at MOI 50 and incubated for a further 2 or 4 h, prior to visualization using differential interference contrast (DIC) and fluorescence microscopy to quantify the percentage of *Burkholderia cenocepacia*-containing vacuoles (BcCVs) colocalizing with TMR-dextran.

For labeling of acidic compartments with LysoTracker Red, RAW264.7 macrophages were infected with bacteria at an MOI of 50. At 4 h postinfection (and immediately prior to visualization by DIC and fluorescence microscopy), acidic compartments within infected macrophages were labeled by incubation with LysoTracker Red DND-99 (Molecular Probes) at a final concentration of 0.25  $\mu$ M for 1 min.

## RESULTS

***Burkholderia* BCP Displays Thiol-Dependent Peroxidase Activity.** Based on homology with known BCP peroxidoredoxins, it was predicted that BcBCP would exhibit thiol-dependent peroxidase activity. N-Terminal 6-His-tagged recombinant WT BcBCP was expressed and purified to homogeneity using a nickel affinity column. Gel filtration of the protein showed it to behave as a monomer with a mass of approximately 19 kDa, which was

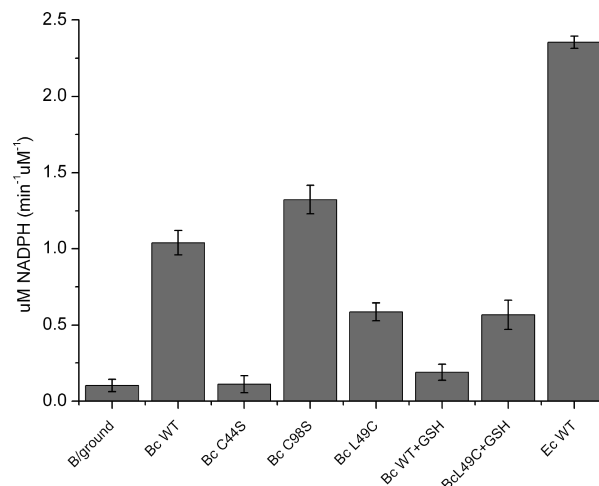


FIGURE 1: Thiol-dependent peroxidase activity of BCP enzymes using thioredoxin as the reducing partner. The thioredoxin-linked peroxidase activity of recombinant BCP proteins was assessed in an assay coupled to the oxidation of NADPH (monitored by a decrease in  $A_{340\text{nm}}$ ) and measured in micromolar NADPH oxidized per minute per micromolar enzyme ( $\mu\text{M min}^{-1} \mu\text{M}^{-1}$ ). The assay contained 0.36  $\mu$ M TrxR, 1.7  $\mu$ M Trx, 0.1 mM  $\text{H}_2\text{O}_2$ , and 0.2 mM NADPH in 50 mM Hepes–NaOH (pH 7). “+GSH” indicated the presence of 1 mM reduced GSH in the reaction mixture. In the absence of BCP, a background (B/ground) level of NADPH oxidation occurs, equating to 0.1  $\mu\text{M min}^{-1}$ . Enzyme activity is stated as the mean of three independent results, and the error bars indicate one standard deviation.

subsequently confirmed by ESI mass spectrometry (average mass 18992 Da).

The peroxidase activity of BcBCP linked to oxidation of NADPH via the *E. coli* thioredoxin/thioredoxin reductase (Trx/TrxR) system was monitored spectrophotometrically by measuring the decrease in  $A_{340\text{nm}}$ . In the absence of BcBCP, a background level of NADPH oxidation occurred at a steady rate of 0.10  $\mu\text{M min}^{-1}$ . In the presence of BcBCP, the rate of NADPH oxidation increased in a BCP concentration-dependent manner and was recorded as  $1.04 \pm 0.08 \mu\text{M min}^{-1} \mu\text{M}^{-1}$  BCP. Comparable BCP enzyme activity was observed in the presence of all peroxide substrates tested (hydrogen peroxide, cumene hydroperoxide, and *tert*-butyl hydroperoxide). Pretreatment of BcBCP with iodoacetamide (IAM; 10 mM final concentration), which covalently modifies free thiol groups, abolished enzyme activity (0.10  $\mu\text{M min}^{-1} \mu\text{M}^{-1}$ ), confirming that the activity of BcBCP is thiol-dependent.

***Cys-44 Is the Active Site of Burkholderia BCP.*** Site-directed mutants of BcBCP were generated, in which each of the cysteine residues was individually replaced with a serine (C44S and C98S BcBCP). The enzymatic activity of these mutants was studied as before. Activity was abolished in the C44S mutant (Figure 1). In contrast, C98S BcBCP retained full enzyme activity. Together, these findings are consistent with the Cys-44 residue being the active site of the thiol-dependent BcBCP, while the Cys-98 residue is a bystander, not involved in the catalytic process. This is consistent with previous observations made of the equivalent cysteine residues (Cys-45 and Cys-99) of EcBCP (2).

The Cys-44 residue of BcBCP was confirmed as the active (peroxidic) cysteine by mass spectrometry (Figure 2). Treatment of WT BcBCP with 10 mol equiv of  $\text{H}_2\text{O}_2$  resulted in an increased mass of 32 Da, consistent with one free thiol group (–SH) being oxidized to the sulfinic acid derivative (–SOOH, Figure 2B). Following treatment with  $\text{H}_2\text{O}_2$ , the mass of C98S

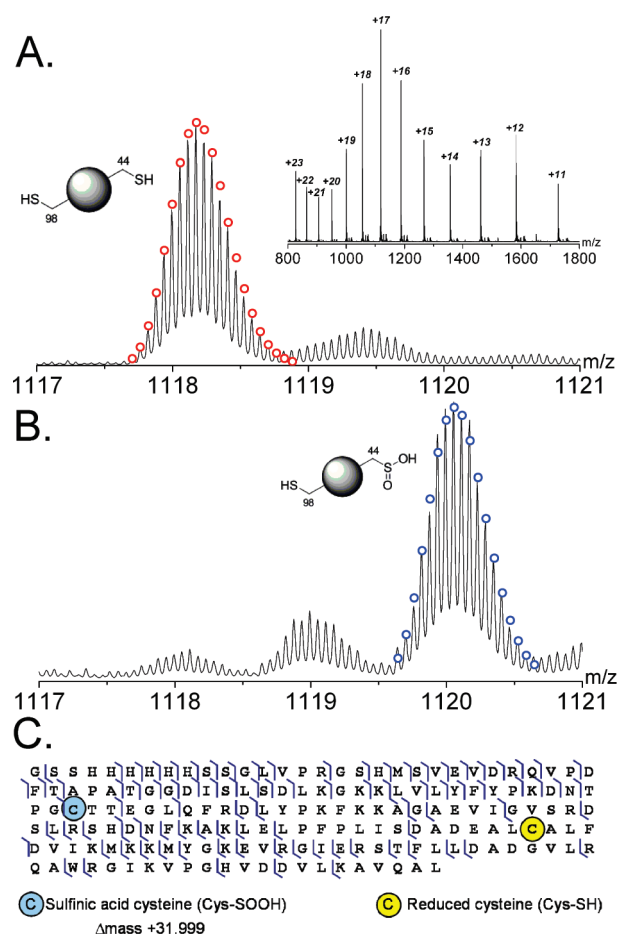


**FIGURE 2:** Mass spectrometry analysis of BcBCP and  $H_2O_2$ -treated BcBCP. BcBCP was analyzed by ESI-FT-ICR-MS in  $H_2O$ –MeOH–HCOOH (50:48:2 v/v/v) at a final concentration of 10  $\mu$ M. (A, insert) A typical spectrum of BcBCP displaying a charge state distribution from  $[M + 11H]^{11+}$  to  $[M + 23H]^{23+}$  and an average deconvoluted mass of 18992 Da. (A) The most abundant ion,  $[M + 17H]^{17+}$ , has an isotope distribution consistent with a theoretical isotope distribution of BcBCP containing two reduced cysteine residues (red circles; empirical formula  $[C_{849}H_{1358}N_{239}O_{246}S_5]^{17+}$ ). (B) BcBCP after addition of 500  $\mu$ M  $H_2O_2$ . The isotope distribution of the  $[M + 17H]^{17+}$  ion reveals a mass shift of +32 Da to an average mass of 19024 Da, which is consistent with the addition of two oxygen atoms, attributed to oxidation of cysteine to sulfinic acid (blue circles; empirical formula  $[C_{849}H_{1358}N_{239}O_{248}S_5]^{17+}$ ). (C) Prosight-PTM output file (cleavage map) showing the top-down fragmentation of sulfinic acid-modified BcBCP. ECD of  $H_2O_2$ -treated BcBCP allowed the modification to be mapped to a three amino acid section containing Cys-44 (see also Supporting Information Figure S1).

BcBCP similarly increased while the mass of C44S BcBCP remained unchanged, suggesting that it is the Cys-44 residue that is oxidized during the catalytic process (data not shown). Top-down fragmentation of the oxidized wild-type enzyme, using ECD, subsequently mapped the sulfinic acid modification to Cys-44, confirming that residue as the peroxidatic cysteine (Figure 2C and Supporting Information Figure S1).

**Burkholderia BCP Is a 1-Cys Peroxiredoxin.** *E. coli* BCP functions via an atypical 2-Cys pathway, employing a peroxidatic cysteine at position 45 and a resolving cysteine at position 50 (3). However, BcBCP lacks the equivalent resolving cysteine (Figure 3). We previously demonstrated that in the absence of the resolving cysteine EcBCP (C50S) adopts a novel mechanistic pathway, progressing via a dimeric intermediate, which contains an intermolecular disulfide bridge between the Cys-45 residues of two monomers (3). The native BcBCP was interrogated by high-resolution mass spectrometry to investigate if it too adopts this novel reaction pathway.

As stated above, in excess  $H_2O_2$  and in the absence of any redox partner, BcBCP forms a stable sulfinic acid (Cys-SOOH), suggesting overoxidation of a sulfenic acid intermediate. However, even at stoichiometric quantities of  $H_2O_2$ , no evidence for dimerization was observed by mass spectrometry. This result led us to speculate whether BcBCP could utilize a small molecule thiol as a resolving partner in a manner previously described for 1-Cys peroxiredoxins (12–16).

A mechanistic study of the 1-Cys D-Prx has highlighted the interaction of glutathione (GSH) with the enzyme during turnover (14). Therefore, experiments with BcBCP were repeated in the presence of 1 mM GSH. Mass spectrometry shows that in the presence of GSH, but absence of  $H_2O_2$ , BcBCP exists as a monomer with two reduced cysteine thiols (Figure 4A). After addition of 1 mol equiv of  $H_2O_2$ , we observed the appearance of a species with  $\Delta$ mass +305 Da, consistent with the formation of a BcBCP-GSH heterodimer (Figure 4B). Presumably, GSH modification is via a mixed disulfide bond with one of the two cysteine residues within BCP. To map the site of glutathionylation, top-down fragmentation was employed. The BcBCP-GSH heterodimer was treated with the alkylating reagent *N*-ethylmaleimide (NEM) to covalently modify any free cysteine thiols. This resulted in an increase of +125 Da, consistent with the alkylation of one cysteine residue. The NEM-labeled GSH-modified species was then reduced by treatment with 20 mM DTT, resulting in a  $\Delta$ mass of –305 Da, which we attribute to loss of GSH. This mass change confirmed that the glutathionylation modification was indeed via a disulfide bond. This final species was subjected to

BcBCP	VSVEVDRQVPDFATGG-DISLSDLKGLVLYFYPKDNTPGCTTEGLQFRDLYPKFK	59
EcBCP	NPLKAGDIAPKFSLPDQDGEQNLITDFQGRVLVYFYPKAMTPGCTVQACGLRDNMDELK	60
BcBCP	KAGAEVIGVSRDLSRSHDNFKAKLELPFPLISDADEALCALFDVIKMKMYGKEVRGIER	119
EcBCP	KAGVDVLGISTDKPEKLSRFABKELLNFTLLSDEDHQVCEQFGVWGBKSFMGKTYDGIHR	120
BcBCP	STFLLDADGVLRQAWRGIVKVPGHVDDVLKAVQAL-	153
EcBCP	ISFLLDADGKIEHVEDDFKTSNHHDDVVLNWLKEHA	155

**FIGURE 3:** Amino acid alignment of *B. cenocepacia* and *E. coli* BCP. BcBCP and EcBCP enzymes have two cysteine residues in common (black arrowheads) at positions Cys-44 and Cys-98 (*B. cenocepacia* coordinates). EcBCP has an additional cysteine at Cys-50 (gray arrowhead) that is not conserved in the *Burkholderia* enzyme. Both amino acid sequences are shown without the N-terminal methionine, which was cleaved from all purified BCP proteins studied.

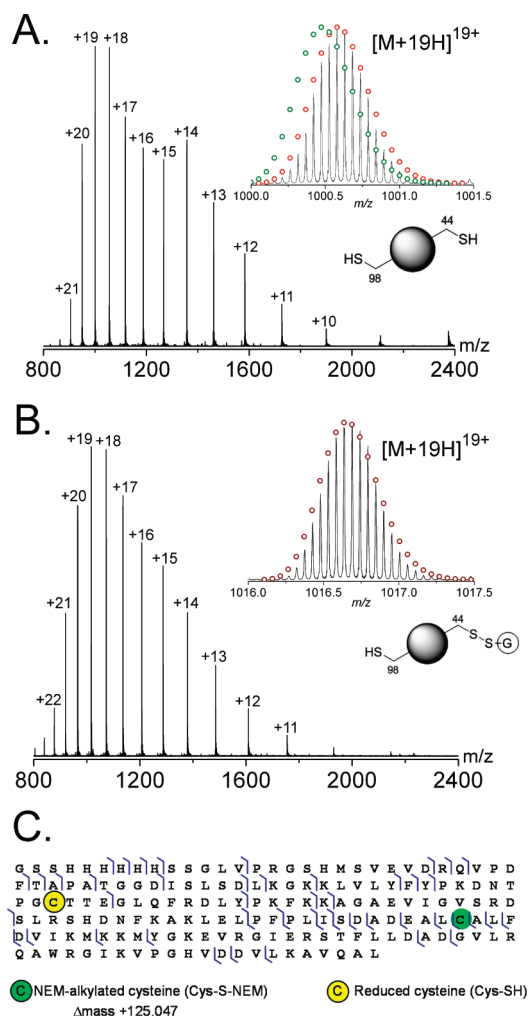


**FIGURE 4:** Glutathione can act as a resolving thiol in *BcBCP* catalysis. *BcBCP* was analyzed by ESI-FT-ICR-MS in H<sub>2</sub>O–MeOH–HCOOH (50:48:2 v/v/v) at a final concentration of 10 μM. (A) Typical mass spectrum of *BcBCP* in the presence of 1 mM GSH. The isotope distribution of the [M + 19H]<sup>19+</sup> charge state is consistent with *BcBCP* containing two reduced cysteine residues (red circles; empirical formula [C<sub>849</sub>H<sub>1360</sub>N<sub>239</sub>O<sub>246</sub>S<sub>5</sub>]<sup>19+</sup>), average deconvoluted mass 18992 Da. For comparison, the theoretical isotope distribution of *BcBCP* containing one disulfide bond ([C<sub>849</sub>H<sub>1358</sub>N<sub>239</sub>O<sub>246</sub>S<sub>5</sub>]<sup>19+</sup>) is shown in green circles. (B) Addition of 1 mol equiv of H<sub>2</sub>O<sub>2</sub> resulted in a second species of average mass 19297 Da (Δmass +305 Da). This species displays an isotope distribution consistent with *BcBCP* containing one reduced cysteine and one glutathionylated cysteine (claret circles; empirical formula [C<sub>859</sub>H<sub>1375</sub>N<sub>242</sub>O<sub>252</sub>S<sub>6</sub>]<sup>19+</sup>). (C) This species was subsequently derivatized with the alkylating agent NEM and reduced with DTT before top-down fragmentation using CID. The Prosight-PTM output file (cleavage map) shows the assignment of the NEM modification to Cys-98, allowing the assignment of the glutathionylated cysteine to Cys-44 (see also Supporting Information Figure S2).

CID fragmentation using FT-ICR-MS. Analysis of the resulting fragments allowed the NEM modification to be mapped to Cys-98, indicating that the glutathionylation occurred on the active cysteine, Cys-44 (Figure 4C and Supporting Information Figure S2).

*Glutaredoxin Can Act as the Reductive Partner to BcBCP in a Glutathione-Dependent Catalytic Pathway.* These mass spectrometric results suggest that GSH acts as a small molecule resolving cysteine, reducing the transient sulfenic acid intermediate on Cys-44 releasing H<sub>2</sub>O and producing a mixed disulfide between Cys-44 and GSH. If this hypothesis is correct, the resulting *BcBCP*-GSH intermediate requires a reductive

partner. This partner must reduce the intermolecular disulfide bond, regenerating a reduced peroxidatic cysteine on *BcBCP*, which would allow further catalytic cycles. Using high-resolution mass spectrometry, we monitored the ability of thioredoxin to reduce the *BcBCP*-GSH intermediate. *BcBCP*-GSH was prepared by treating reduced *BcBCP* with 2 equiv of H<sub>2</sub>O<sub>2</sub> in the presence of 1 mM GSH (as shown in Figure 4B). Excess GSH and peroxide were removed using size exclusion chromatography before this species was incubated with an equimolar ratio of reduced thioredoxin. The mixture was equilibrated at room temperature for 2 min before analysis by FT-ICR-MS (Supporting Information Figure S3). Analysis of the isotopic distributions within the resulting mass spectrum revealed no mass shift for either species, suggesting that thioredoxin is not an efficient reducing partner for *BcBCP*-GSH. This observation seemed to contradict results from the Trx/TrxR enzyme assay that demonstrated enzyme turnover using thioredoxin as the reducing partner. However, repeating the enzyme assay in the presence of 1 mM GSH resulted in a dramatic loss of enzyme activity, recorded at  $0.19 \pm 0.05 \mu\text{M min}^{-1} \mu\text{M}^{-1}$  (Figure 1). This result suggests that glutathionylation of the peroxidatic cysteine inhibits the thioredoxin-dependent reductive step of catalysis. Together, these observations imply that thioredoxin can act as a reductant in *BcBCP* catalysis by *directly* reducing the transient Cys-44-S-OH intermediate to Cys-44-SH. However, in the presence of GSH, the transient Cys-44-S-OH is quickly glutathionylated. The resulting *BcBCP*-GSH mixed disulfide is not a substrate for reduction by thioredoxin, and *BcBCP* turnover is inhibited.

As stated above, glutathione-dependent catalysis has been reported previously for peroxiredoxin enzymes: the poplar phloem 1-Cys D-Prx has been extensively studied and displays glutathione dependence (15, 16). Furthermore, NMR and MS studies of this enzyme have revealed that the poplar Prx can be glutathionylated on its peroxidatic cysteine residue and the enzyme accepts glutaredoxin (Grx) as a proton donor (14). Using high-resolution MS, we monitored the ability of glutaredoxin to reduce the *BcBCP*-GSH intermediate. Equimolar ratios of reduced Grx and *BcBCP*-GSH were mixed and equilibrated at room temperature for 2 min. After allowing the reaction to proceed, FT-ICR-MS analysis revealed that Grx displayed a Δmass of –2 Da, consistent with oxidation of Grx and formation of an intramolecular disulfide bond, and the *BcBCP* species underwent a mass shift of –305 Da, consistent with reduction of the glutathione moiety, and displayed an isotope distribution consistent with *BcBCP* containing two reduced cysteines (Figure 5). This result indicates that Grx can efficiently reduce the *BcBCP*-GSH mixed disulfide.

In light of these mass spectrometric results, *BcBCP* was assayed for peroxiredoxin activity using an NADPH-linked GSH/Grx/glutathione reductase system and was monitored spectrophotometrically by measuring the decrease in A<sub>340nm</sub>. As expected, NADPH oxidation was observed in the presence of BCP, and activity increased in a BCP concentration-dependent manner (Figure 6). *BcBCP* displayed an activity of  $6.10 \pm 0.04 \mu\text{M min}^{-1} \mu\text{M}^{-1}$  and was dependent on the presence of Grx and GSH in the reaction. Interestingly, this activity is greater than 5-fold higher than the activity using Trx/TrxR as a reducing system under similar conditions.

*Introduction of Cys-49 Converts Burkholderia BCP to an Atypical 2-Cys Prx.* To investigate the differences between the *E. coli* and *Burkholderia* BCP homologues, a resolving



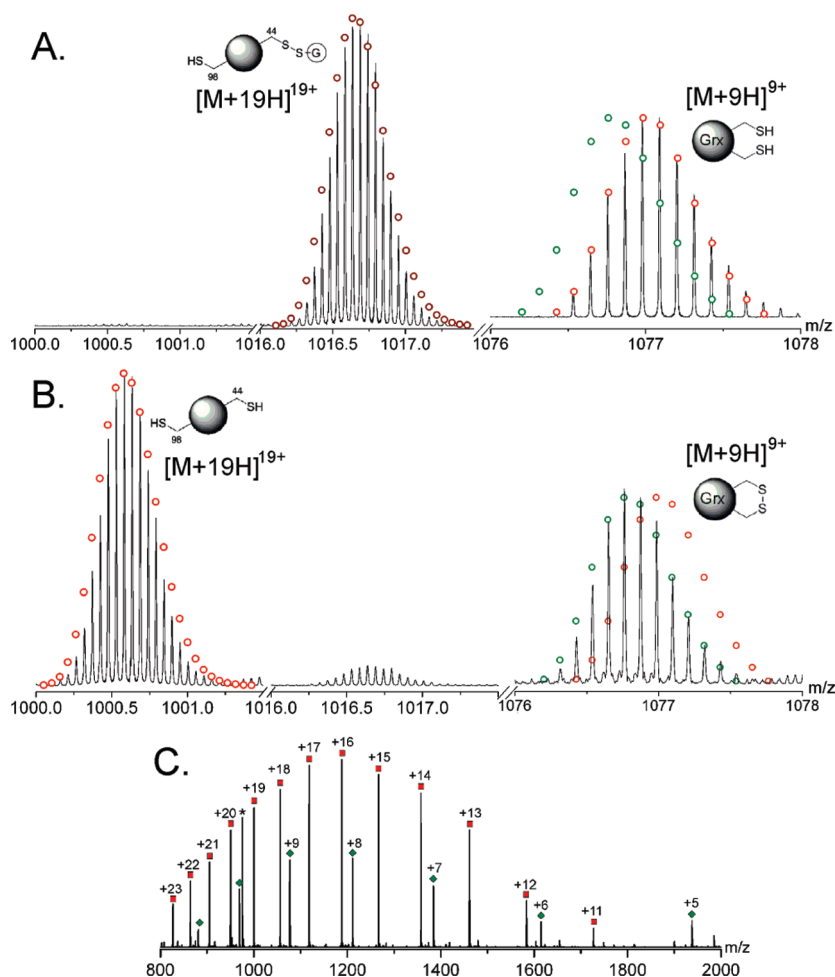


FIGURE 5: Analysis of potential reductive partners for *BcBCP* catalysis using mass spectrometry. Glutaredoxin can efficiently reduce glutathionylated *BcBCP*. An equimolar mixture of *BcBCP*-GSH and reduced Grx was incubated at room temperature for 2 min before being quenched with  $\text{H}_2\text{O}$ -MeOH- $\text{HCOOH}$  (50:48:2 v/v/v). The resulting mixture was analyzed by FT-ICR-MS at a final protein concentration of  $10\ \mu\text{M}$ . (A) Analysis of the isotope distributions of *BcBCP*-GSH and Grx before mixing. *BcBCP*-GSH displays an isotope distribution consistent with the glutathionylated protein (claret circles;  $[\text{C}_{859}\text{H}_{1375}\text{N}_{242}\text{O}_{252}\text{S}_6]^{19+}$ ). The  $[\text{M} + 9\text{H}]^{9+}$  charge state of the glutaredoxin species displayed an isotope distribution consistent with reduced Grx (red circles;  $[\text{C}_{429}\text{H}_{671}\text{N}_{116}\text{O}_{134}\text{S}_3]^{9+}$ ). The theoretical isotope distribution of oxidized Grx is shown in green circles for comparison ( $[\text{C}_{429}\text{H}_{669}\text{N}_{116}\text{O}_{134}\text{S}_3]^{9+}$ ). (B) Analysis of the isotope distributions of *BcBCP* and Grx after mixing. The *BcBCP* species displays an isotope distribution consistent with the reduced protein, indicating loss of the GSH moiety (red circles;  $[\text{C}_{849}\text{H}_{1360}\text{N}_{239}\text{O}_{246}\text{S}_5]^{19+}$ ). The  $[\text{M} + 9\text{H}]^{9+}$  charge state of the glutaredoxin species displayed an isotope distribution consistent with oxidized Grx (green circles;  $[\text{C}_{429}\text{H}_{669}\text{N}_{116}\text{O}_{134}\text{S}_3]^{9+}$ ) consistent with the formation of a disulfide bond. (C) Broad-band mass spectrum showing the charge state distributions of reduced *BcBCP* and oxidized Grx. BCP charge states are indicated by red squares; Grx charge states are indicated by green triangles.

cysteine was introduced into *BcBCP* (L49C) at an equivalent position to the resolving cysteine of the *E. coli* enzyme (Cys-50).

The activity and catalytic mechanism of L49C *BcBCP* were examined by mass spectrometry. Oxidation of L49C *BcBCP* with  $\text{H}_2\text{O}_2$  resulted in a  $\Delta\text{mass}$  of  $-2\ \text{Da}$ , which we attribute to the loss of two hydrogen atoms, consistent with the formation of an intramolecular disulfide bond between two cysteines (Figure 7A,B). This disulfide bond was formed upon treatment with peroxide both with and without the presence of  $1\ \text{mM}$  GSH. Disulfide bond formation was confirmed by treatment of the oxidized protein with NEM, which resulted in the modification of only a single thiol group (data not shown). The site of NEM modification was examined by top-down fragmentation. CID fragmentation revealed that Cys-98 was modified by NEM and that Cys-44 and Cys-49 formed the intramolecular disulfide bond (Figure 7C and Supporting Information Figure S4). Together, these results demonstrate that the L49C *BcBCP* mutant acts via the atypical 2-Cys Prx mechanism, in a manner similar to *EcBCP*.

Having demonstrated by MS that L49C *BcBCP* functions as an atypical 2-Cys Prx, we investigated the activity of the enzyme using the previously described enzyme assays. Although less active than the wild-type enzyme, L49C *BcBCP* displays an activity of  $0.59 \pm 0.06\ \mu\text{M}\ \text{min}^{-1}\ \mu\text{M}^{-1}$  using Trx/TrxR as the reductive partners (Figure 1), confirming that the Cys-44–Cys-49 intramolecular disulfide bond can be resolved by the Trx/TrxR redox system. This activity was not inhibited by the presence of GSH. L49C BCP was also compared to the native *E. coli* enzyme, as the catalytic mechanism of these enzymes appears to be identical by MS. The activity of the native *E. coli* enzyme was 4-fold greater than that of L49C *BcBCP* (Figure 1). Indeed, *EcBCP* displayed greater activity than all isoforms of *BcBCP* (WT and site-directed mutants) using this assay with Trx/TrxR as the reductive partners (Figure 1).

Analyzing the activity of the *BcBCP* L49C using the GSH/Grx system, we found that introduction of the cysteine resulted in an activity of  $0.47 \pm 0.09\ \mu\text{M}\ \text{min}^{-1}\ \mu\text{M}^{-1}$ , a 15-fold decrease in comparison to wild-type *BcBCP* (Figure 6). We also assayed the

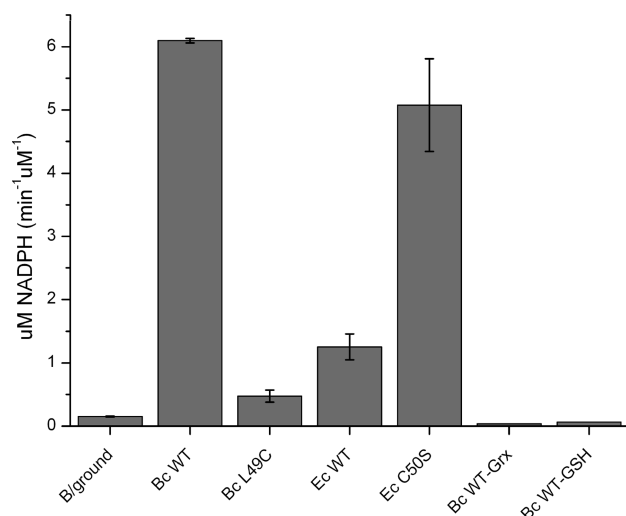


FIGURE 6: Peroxidase activity of BCP enzymes using glutaredoxin as the reducing partner. The GSH/glutaredoxin-linked peroxidase activities of recombinant BCP proteins were assessed in an assay coupled to the oxidation of NADPH (monitored by a decrease in  $A_{340\text{nm}}$ ) and measured in micromolar NADPH oxidized per minute per micromolar enzyme ( $\mu\text{M min}^{-1} \mu\text{M}^{-1}$ ). The assay contained 1 unit of glutathione reductase, 12  $\mu\text{M}$  Grx, 1 mM GSH, 0.1 mM hydrogen peroxide, and 0.15 mM NADPH in 50 mM Hepes–NaOH (pH 7). Enzyme activity is stated as the mean of three independent results, and the error bars indicate one standard deviation.

activity of WT *EcBCP* using this assay. Again, this enzyme showed significantly lower activity than WT *BcBCP* (Figure 6). These results suggest that the GSH/Grx system is not an efficient reducing partner for peroxidoredoxins that catalyze peroxide reduction via the 2-Cys mechanism. Presumably this system cannot reduce the intramolecular disulfide formed in the reaction pathway of these enzymes. To test this hypothesis, the redox exchange reaction between oxidized *BcBCP* L49C and reduced glutaredoxin/GSH was monitored by MS. An equimolar mixture of oxidized *BcBCP* L49C and reduced glutaredoxin was allowed to equilibrate for 2 min in the presence of 1 mM GSH, before analysis by FT ICR-MS. As expected, analysis of the isotopic abundances within the resulting mass spectrum revealed that both species were unchanged (Supporting Information Figure S5, top), highlighting the inability of Grx/GSH to reduce the Cys-44–Cys-49 disulfide bond within *BcBCP* L49C. In a similar experiment, no reduction of oxidized wild-type *EcBCP* by Grx/GSH was observed by FT-ICR-MS (data not shown). In contrast, MS analysis of the redox exchange reaction between *BcBCP* L49C and reduced thioredoxin demonstrates that thioredoxin can reduce oxidized *BcBCP* L49C. However, it is interesting to note that to fully reduce *BcBCP* L49C, thioredoxin was added in 5-fold molar excess (Supporting Information Figure S5, bottom). These MS results correlate with the enzyme assay results (presented here and in ref 3), which suggest that Trx is the preferred redox partner for the 2-Cys Prxs *EcBCP* and *BcBCP* L49C.

**The *Burkholderia bcp* Gene Shows Unique Linkage and Coexpression with the *arn* Locus.** We previously reported that the gene encoding *BcBCP* (BCAL1936; *B. cenocepacia* J2315 gene nomenclature) is coexpressed with the *arn* locus (BCAL1929-1935) (7). Here, we further investigated this intriguing linkage of two different, but complementary, resistance determinants through comparative genomic analyses and quantitative gene expression studies.

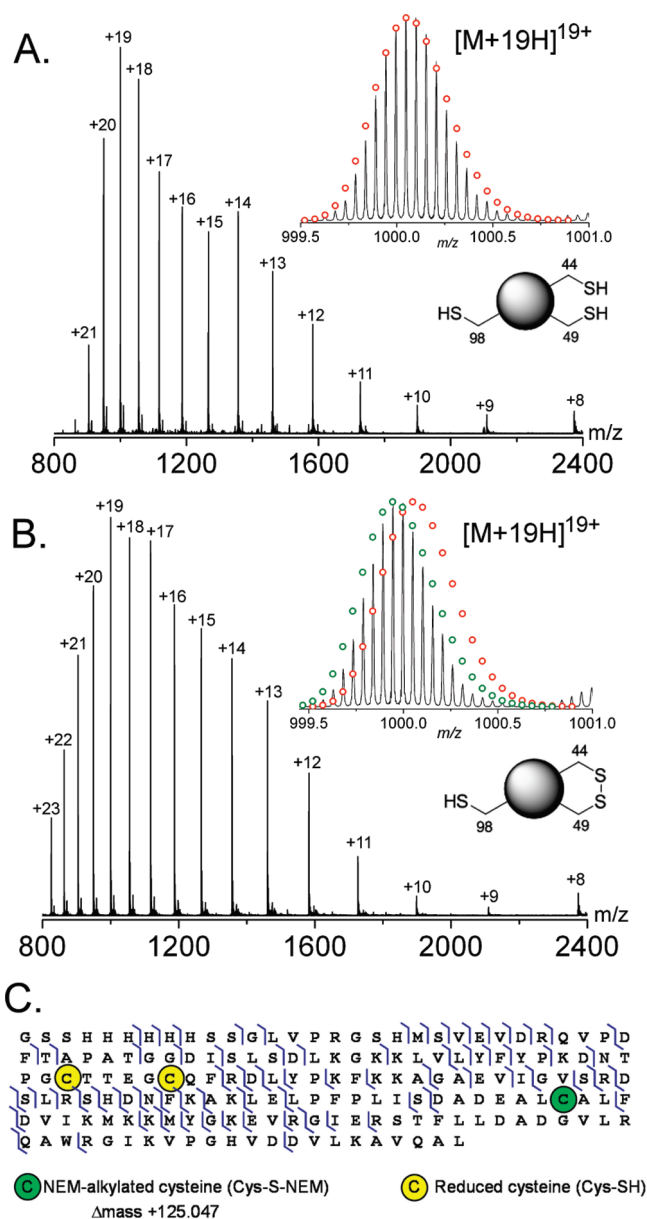


FIGURE 7: Introduction of a resolving cysteine (L49C) converts *BcBCP* from a 1-Cys Prx to an atypical 2-Cys Prx. *BcBCP* L49C was analyzed by ESI-FT-ICR-MS in  $\text{H}_2\text{O}$ – $\text{MeOH}$ – $\text{HCOOH}$  (50:48:2 v/v/v) at a final concentration of 10  $\mu\text{M}$ . (A) Typical mass spectrum of L49C *BcBCP* displaying a charge state distribution from  $[\text{M} + 8\text{H}]^{8+}$  to  $[\text{M} + 21\text{H}]^{21+}$  and an average mass of 18982 Da. Analysis of the isotope distribution of the  $[\text{M} + 19\text{H}]^{19+}$  charge state reveals a distribution consistent with L49C *BcBCP* containing three reduced cysteines (red circles; empirical formula  $[\text{C}_{846}\text{H}_{1354}\text{N}_{239}\text{O}_{246}\text{S}_6]^{19+}$ ). (B) The mass spectrum of L49C *BcBCP* after addition of 1 mol equiv of  $\text{H}_2\text{O}_2$ , in the presence of 1 mM GSH, displays a charge state distribution from  $[\text{M} + 8\text{H}]^{8+}$  to  $[\text{M} + 17\text{H}]^{17+}$ . The isotope distribution of the  $[\text{M} + 19\text{H}]^{19+}$  reveals a  $\Delta\text{mass}$  of  $-2$  Da and is consistent with L49C *BcBCP* containing one disulfide bond and one reduced cysteine (green circles; empirical formula  $[\text{C}_{846}\text{H}_{1352}\text{N}_{239}\text{O}_{246}\text{S}_6]^{19+}$ ). (C)  $\text{H}_2\text{O}_2$ -treated L49C *BcBCP* was subsequently derivatized with the alkylating agent NEM and reduced with DTT before top-down fragmentation using ECD. The Prosight-PTM output file (cleavage map) shows the assignment of the NEM modification to Cys-98, allowing the assignment of the disulfide bond to Cys-44 and Cys-49 (see also Supporting Information Figure S4).

Analysis of publicly available genomes that contain a *bcp* homologue revealed that the linkage of *bcp* with the *arn* locus is unique to  $\beta$ -proteobacteria that exhibit innate resistance to the polymyxin class of antimicrobials (*Burkholderia* species and the



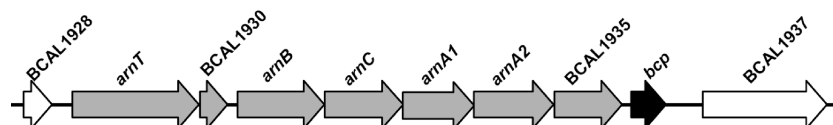


FIGURE 8: Genetic linkage of *bcp* in the genus *Burkholderia*. Within  $\beta$ -proteobacteria that exhibit innate resistance to cationic antimicrobial peptides (*Burkholderia* species and organisms of the *R. pickettii* group) *bcp* (black arrow) is located immediately downstream of the *arm* locus (gray arrows). The flanking genes BCAL1928 and BCAL1937 (white arrows) encode a hypothetical protein and a PhoH-like protein, respectively. "BCAL" gene nomenclature refers to the genome sequence of *B. cenocepacia* J2315, chromosome 1.

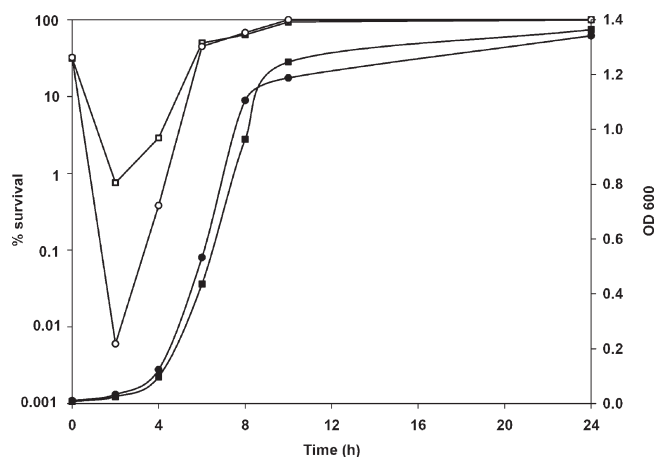


FIGURE 9: Growth-phase-dependent role of *BcBCP* in protecting against oxidative stress. At regular intervals throughout the growth phase, percentage survival of *B. cenocepacia* K56-2 and the BCP-deficient strain XOA14 was assessed following challenge of each strain with 1 mM  $\text{H}_2\text{O}_2$  for 30 min. Both K56-2 and XOA14 showed comparable growth in aerobic conditions (closed squares and closed circles, respectively). XOA14 is hypersensitive to  $\text{H}_2\text{O}_2$ -mediated killing at lag phase/early log phase of growth (open circles), compared to K56-2 (open squares). At stationary phase, both strains are equally resistant to  $\text{H}_2\text{O}_2$ -mediated killing.

closely related *Ralstonia pickettii* lineage). The genetic organization of the locus is shown in Figure 8. In the majority of polymyxin-sensitive  $\beta$ -proteobacteria studied, including *Bordetella*, *Comamonas*, and *Delftia* species, the *bcp* gene is flanked by homologues of BCAL1928 and BCAL1937 without the intervening *arm* locus. In contrast, in  $\gamma$ -proteobacteria (including *Salmonella*, *Shigella*, and *Pseudomonas* species), there is conserved linkage of the *bcp* and *gcvR* genes, the latter coding for the glycine cleavage repressor protein (17). This is consistent with the previous report that the *E. coli bcp* gene is located immediately downstream of the *gcvR* gene, but expressed independently (18). It should be noted that  $\beta$ -proteobacteria generally do not possess orthologues of *GcvR* (19).

Northern blot analysis of *B. cenocepacia* K56-2 at logarithmic phase revealed the presence of an abundant *bcp* transcript of approximately 830 bp, suggesting that *bcp* is strongly expressed independently, in addition to its previously described coexpression with the *arm* locus (7). We previously reported that the *Burkholderia arm* locus is expressed as two transcriptional units. Consequently, the independent expression of *bcp* was investigated further by QRT-PCR, comparing the level of *bcp* expression with that of representative genes from each transcriptional unit of the *arm* locus (*armT* and *armB*). The abundance of *bcp* transcript was approximately 11-fold higher than both *armT* and *armB* (Supporting Information Figure S6), confirming the strong independent expression of *bcp*. A comparable ratio of transcripts was observed irrespective of the growth phase studied (data not shown).

*Burkholderia BCP Confers Growth-Phase-Dependent Resistance to Oxidative Killing.* Insertional inactivation of the *bcp* gene in *B. cenocepacia* K56-2 resulted in strain XOA14. To explore the role of *BcBCP*, the sensitivity of K56-2 and XOA14 to oxidative killing was assessed at regular time points throughout the growth phase. As shown in Figure 9, XOA14 is hypersensitive to  $\text{H}_2\text{O}_2$ -mediated killing; however, this hypersensitivity is restricted to the lag phase/early log phase of growth. At stationary phase, there is no difference in the survival of XOA14 and K56-2 following treatment with  $\text{H}_2\text{O}_2$ . The hypersensitivity of XOA14 to oxidative killing at lag phase could be rescued through complementation with WT *BcBCP* encoded on plasmid pARB10 (Supporting Information Figure S7).

*Burkholderia BCP Is Not Required for Intracellular Survival.* Having demonstrated hypersensitivity to oxidative killing, the ability of XOA14 to survive within macrophages was assessed and compared with K56-2. Cumulative evidence suggests that Bcc do not actively replicate intracellularly (20, 21). Consequently, we consider the use of stationary phase bacteria to be most physiologically relevant for Bcc intracellular survival assays. However, given the growth-phase-dependent hypersensitivity of XOA14 to peroxide-mediated killing, we investigated intracellular survival and/or intracellular localization using both early log phase and stationary phase bacteria.

As shown in Figure 10A, intracellular survival of early log phase XOA14 is no different from that of K56-2, suggesting that the role of *BcBCP* is to protect from oxidative stresses in the extracellular rather than intracellular environment. Stationary phase bacteria were then used to compare the localization of K56-2 and XOA14 within macrophages (Figure 10B). The persistence of Bcc within macrophages in the apparent absence of replication has been associated with their ability to delay the maturation of the phagosome, persisting instead within *B. cepacia*-containing vacuoles (BcCVs) (for review, see ref 22). Key events in the maturation of phagosomes include their progressive acidification and ultimately fusion with lysosomes. These processes can be monitored using LysoTracker Red and TMR-dextran, which (when visualized by fluorescence microscopy) label acidic organelles and lysosomes, respectively. Microscopy of infected macrophages allows BcCVs to be visualized, and the percentage of BcCVs colocalizing with either LysoTracker Red or TMR-dextran can be calculated. A strain that is impaired in its ability to persist intracellularly (by delaying phagosomal maturation) would be expected to yield a higher proportion of LysoTracker Red- and/or TMR-dextran-colocalizing BcCVs. The BCP-deficient XOA14 displays a marginally higher proportion of LysoTracker Red- and TMR-dextran-colocalizing BcCVs 4 h postinfection compared to K56-2, but these differences are not statistically significant (Figure 10B). Therefore, we conclude that *BcBCP* is not critical for the intracellular survival of *B. cenocepacia* in murine macrophages.

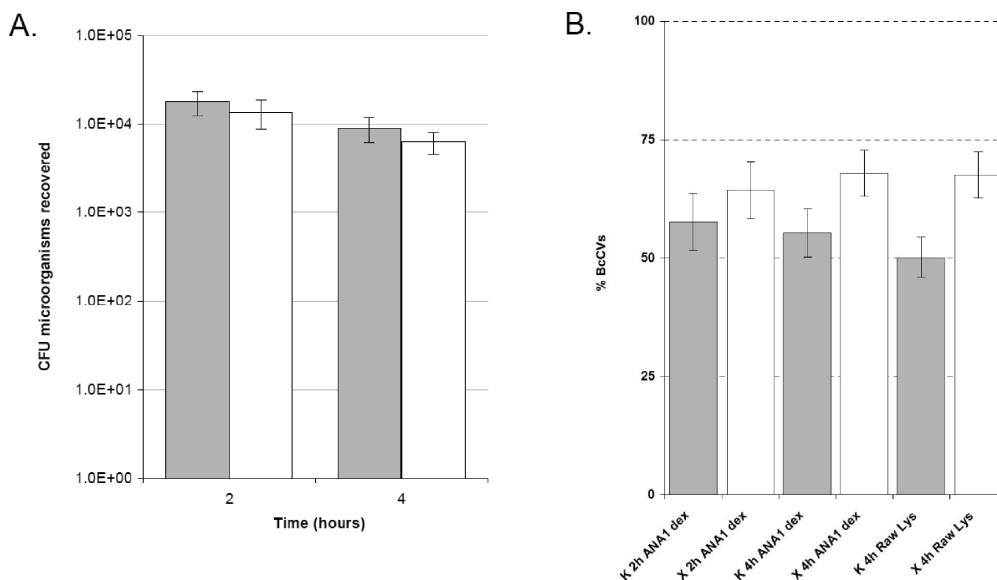


FIGURE 10: Comparison of intracellular survival and localization within murine macrophages of *B. cenocepacia* K56-2 and the BCP-deficient XOA14. Macrophage infection assays demonstrate that *Burkholderia* BCP is not required for intracellular survival. (A) Intracellular survival of early log phase *B. cenocepacia* K56-2 (gray bars) and XOA14 (white bars) was quantified 2 and 4 h postinfection (MOI 50). The BCP-deficient XOA14 is not impaired in intracellular survival at early log phase relative to K56-2. (B) The number of *B. cenocepacia*-containing vacuoles (BcCVs) colocalizing with either TMR-dextran (dex) or LysoTracker Red (Lys) was compared following either 2 or 4 h infection of murine macrophages (ANA1 or Raw264.7) with stationary phase K56-2 (gray bars, “K”) or XOA14 (white bars, “X”). The number of BcCVs colocalizing with TMR-dextran or LysoTracker Red is not significantly different when comparing the two strains, indicating that the stationary phase BCP-deficient XOA14 is not impaired in its ability to persist within macrophages.

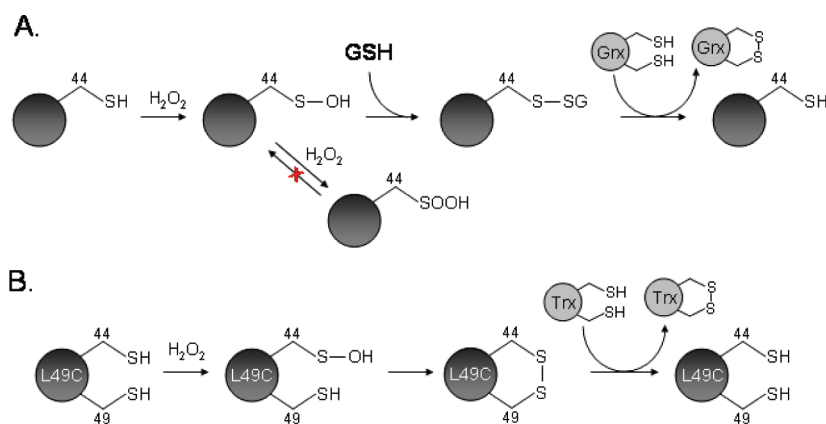


FIGURE 11: Schematic depiction of the peroxidatic mechanisms of 1-Cys and atypical 2-Cys BCPs. (A) Catalytic mechanism of a 1-Cys BCP, as exemplified by wild-type *BcBCP*. The enzyme functions via a GSH/Grx-dependent 1-Cys Prx mechanism. In the presence of peroxide, the peroxidatic cysteine (Cys-44) is oxidized to a sulfenic acid intermediate. In the absence of a small molecule thiol, this sulfenic acid intermediate is irreversibly oxidized to sulfinic acid. However, in the presence of glutathione (GSH), a *BcBCP*-GSH heterodimer is formed, which is subsequently resolved by reduced glutaredoxin. (B) Catalytic mechanism of an atypical 2-Cys BCP, as exemplified by L49C *BcBCP* or *EcBCP*. The peroxidatic cysteine is oxidized to the sulfenic acid intermediate prior to disulfide bond formation with the resolving cysteine (Cys-49). The formation of this intramolecular disulfide bond is highly favored, occurring even in the presence of excess GSH. The disulfide bridge between Cys-44 and Cys-49 can be resolved by the Trx/TrxR redox system.

## DISCUSSION

BCP is a thiol-dependent Prx of the AhpC/TSA family that is present in diverse bacterial species. Recently, we reclassified *EcBCP*, the founder member of this group of enzymes, as an atypical 2-Cys Prx on the basis of high-resolution MS analysis (3). In the present study, we describe the BCP of *B. cenocepacia*, a novel member of the BCP family and an addition to the repertoire of “superoxide detoxification” gene products recently identified within the *B. cenocepacia* J2315 genome (23). We provide the first detailed characterization of the 1-Cys BCP-peroxidatic mechanism and demonstrate that BCP homologues fall into one of two functional groups, based on the presence or absence of a resolving cysteine (Figure 11). In the presence of the resolving cysteine, as

typified by *EcBCP*, the sulfenic acid intermediate that forms following oxidation of the peroxidatic cysteine is rapidly reduced through the formation of an intramolecular disulfide bond with the resolving cysteine (atypical 2-Cys Prx mechanism). Crucially, this occurs even in the presence of excess GSH (3), indicating that in the presence of the resolving cysteine the formation of the intramolecular disulfide bond is strongly favored over the formation of a BCP-GSH heterodimer. This intramolecular disulfide bond is subsequently reduced by thioredoxin, completing the catalytic cycle. In contrast, *BcBCP* described in the present study lacks the resolving cysteine. This enzyme displays moderate enzymatic activity using thioredoxin, presumably with Trx directly reducing the sulfenic acid intermediate. However, here

we demonstrate that in the presence of GSH this Trx-dependent catalysis is inhibited. Furthermore, the enzyme forms a rapid BCP-GSH heterodimer following oxidation of the peroxidatic cysteine, in a manner previously described by Noguera-Mazon et al. (14). We show that this resolving complex is not a substrate for reduction by thioredoxin, but by the redox partner glutaredoxin. Introduction of a resolving cysteine (L49C) converts the *Burkholderia* enzyme to an atypical 2-Cys Prx that can be reduced by thioredoxin, thus retaining enzyme activity. A schematic of the WT and L49C *BcBCP* reaction mechanisms is shown in Figure 11.

BCP homologues found in the majority of bacterial species lack the equivalent of the *EcBCP* resolving cysteine (Cys-50) (Supporting Information Figure S8 and ref 3). Of 59 BCP proteins represented in Figure S8, only 18 have a cysteine residue at the equivalent position of the *E. coli* Cys-50, and these 18 BCP homologues are almost exclusively found in a restricted set of  $\gamma$  proteobacteria. The majority of bacterial BCP homologues, from taxonomically diverse bacterial species, lack an apparent resolving cysteine and are presumed to exhibit the 1-Cys mechanism, typified by the native *Burkholderia* enzyme.

We previously reported that the engineered C50S *EcBCP* retains activity through a novel catalytic mechanism that is distinct from the 1-Cys pathway (3). In contrast, we have demonstrated in the current study that the native *BcBCP* that lacks the equivalent resolving cysteine functions via a GSH/Grx-dependent 1-Cys pathway. We also assessed the activity of the *EcBCP* C50S mutant in the Grx assay (Figure 6). This single-cysteine BCP mutant displays activity approaching the level of *BcBCP* in this assay, suggesting it can also act via a BCP-GSH mixed disulfide resolving complex. In our previous study, MS analysis of the *EcBCP* C50S was performed without the presence of GSH. MS analysis of this enzyme after oxidation with peroxide was repeated in the presence of 1 mM GSH and revealed a mixture of both BCP-GSH and BCP-BCP mixed disulfide dimers (data not shown). Thus, it seems that two resolving pathways can be used by this BCP variant. In contrast, no evidence for intermolecular disulfide bond formation and BCP dimers was found for WT *BcBCP*. Comparison of the amino acid sequences of representative BCP homologues shows that in atypical 2-Cys enzymes that possess an equivalent resolving cysteine to *EcBCP* (Cys-50), the conserved region that encompasses the peroxidatic cysteine extends up to (and beyond) the resolving cysteine (Supporting Information Figure S9). In contrast, BCP homologues that lack the resolving cysteine are divergent after the active TPGCT motif. It may be that these differences in amino acid sequence and thus architecture around the peroxidatic cysteine account for the subtle differences observed between the engineered C50S *EcBCP* enzyme and the native *Burkholderia* enzyme. There may be merit in high-resolution 3D structural studies of these BCPs to further explore the link between these isoform-specific sequence differences and catalytic mechanism. Such studies of the BCP homologue of *Xanthomonas campestris* (*XcBCP*) have recently been reported (24). While *XcBCP* possesses a resolving cysteine and functions as an atypical 2-Cys Prx, it differs from *EcBCP* in the positioning of the resolving cysteine relative to the peroxidatic cysteine. The peroxidatic and resolving cysteines of *EcBCP* (Cys-45 and Cys-50, respectively) are present within the same  $\alpha$ -helix, but the equivalent cysteines of *XcBCP* (Cys-48 and Cys-84, respectively) are in different  $\alpha$ -helices (24). Consequently, the proposed pathway of alternate opening and closing of the

substrate entry channel and disulfide bond pocket in *XcBCP* (24) is unlikely to be directly applicable to the *E. coli* enzyme or, indeed, the 1-Cys *BcBCP*. Equivalent studies of the *EcBCP* and *BcBCP* homologues are required to establish the structural changes that occur in the catalytic cycles of these 1-Cys and 2-Cys BCP variants.

The BCP-associated phenotype shows variation between different bacterial species. While BCP-deficient *B. cenocepacia* and *E. coli* (2) are hypersensitive to hydrogen peroxide, BCP-deficient *Helicobacter pylori* are not (25). This variable phenotype is most likely a consequence of differences in the repertoire and relative abundance of other antioxidant proteins within the cell. In the case of *H. pylori*, the 2-Cys AhpC peroxidase is considerably more abundant than BCP. Consequently, an *ahpC*-deficient *H. pylori* mutant is significantly more sensitive to oxidative killing than the *bcp*-deficient mutant (25). Indeed, given that we observed consistent expression (at the transcript level) of *bcp* throughout the growth phase of *B. cenocepacia*, we believe that the growth-phase-dependent phenotype of the BCP-deficient strain XOA14 is a consequence of other antioxidant factors being strongly induced at late exponential/stationary phase, thus rendering *BcBCP* essentially redundant. Several antioxidants identified within the Bcc as playing a decisive role in intracellular survival show dramatically increased activities at stationary phase, including superoxide dismutase (SodC), catalase enzymes (including the bifunctional catalase-peroxidase, KatB), and a melanin-like pigment (26–29). Similarly, an apparent AhpC-deficient variant of *B. cenocepacia* C1394 is hypersensitive to oxidative killing at stationary phase relative to the parent strain (30). In *B. cenocepacia*, we propose that the Prx activity of BCP fulfils a protective role under physiological conditions that precede the induction of these stationary phase antioxidants and that this protective role is restricted to the extracellular environment under conditions that favor active bacterial replication. It has been established that intracellular *B. cenocepacia* only minimally replicates in macrophages (21, 31). Therefore, it is possible that *BcBCP* antioxidant activities are physiologically relevant in actively metabolic bacteria, as has been observed for the *B. cenocepacia* KatA protein that is required for antioxidant protection of enzymes of the TCA cycle (29). How *BcBCP* activity, and indeed that of other antioxidants, contributes to the survival of *B. cenocepacia* within the specific environment of the CF lung is unclear. Intriguingly, *Pseudomonas aeruginosa* isolates from CF infants show reduced expression of *bcp* relative to that observed in the wound isolate, and common laboratory strain, PAO1 (R. K. Ernst, personal communication). Furthermore, loss of the related antioxidant AhpC in *B. cenocepacia* has been associated with the ability to establish persistent pulmonary infection in a murine host (30). This latter observation suggests that *Burkholderia* AhpC may be immunogenic, as has been observed for *Salmonella typhimurium* AhpC (32). The immunogenicity of BCP has yet to be addressed, and further studies are required to establish the role that these bacterial antioxidants play in the adaptation to CF airways.

In conclusion, we have described a novel Prx enzyme of *Burkholderia* and characterized its catalytic activity. Although *BcBCP* does not appear to play a pivotal role in the intracellular survival of *B. cenocepacia*, it confers resistance to ROS at a time when other known antioxidant mediators are not expressed, or expressed only at a low level. While homologous to the previously described atypical 2-Cys BCP peroxidase of *E. coli*, the *Burkholderia* enzyme lacks the resolving cysteine and functions via a



1-Cys peroxidatic mechanism utilizing an external small molecule thiol redox partner, glutathione, to resolve the oxidized peroxidatic cysteine. The resulting glutathionylated BcBCP intermediate is subsequently reduced by glutaredoxin. These studies provide the first detailed characterization of the 1-Cys Prx pathway in a BCP, highlight the mechanistic differences that exist within the BCP family of bacterial peroxidoredoxins, and support their subdivision into two classes based on their catalytic activity.

## SUPPORTING INFORMATION AVAILABLE

Top-down fragmentation of H<sub>2</sub>O<sub>2</sub>-treated WT BcBCP, NEM-modified WT BcBCP, and NEM-modified L49C BcBCP; MS analysis of the reduction of BcBCP-GSH heterodimer by thioredoxin; MS analysis of the reduction of oxidized BcBCP L49C by glutaredoxin and thioredoxin; quantitative RT-PCR analysis of *bcp* expression; complementation of BCP-deficient *B. cenocepacia* XOA14 with WT BcBCP; phylogenetic tree of bacterial BCP homologues; amino acid alignments of representative BCP homologues with and without the resolving cysteine. This material is available free of charge via the Internet at <http://pubs.acs.org>.

## REFERENCES

- Poole, L. B. (2007) The catalytic mechanisms of peroxidoredoxins. *Subcell. Biochem.* 44, 61–81.
- Jeong, W., Cha, M. K., and Kim, I. H. (2000) Thioredoxin-dependent hydroperoxide peroxidase activity of bacterioferritin comigratory protein (BCP) as a new member of the thiol-specific antioxidant protein (TSA)/alkyl hydroperoxide peroxidase C (AhpC) family. *J. Biol. Chem.* 275, 2924–2930.
- Clarke, D. J., Mackay, C. L., Campopiano, D. J., Langridge-Smith, P., and Brown, A. R. (2009) Interrogating the molecular details of the peroxidoredoxin activity of the *Escherichia coli* bacterioferritin comigratory protein using high-resolution mass spectrometry. *Biochemistry* 48, 3904–3914.
- Mahenthalingam, E., Urban, T. A., and Goldberg, J. B. (2005) The multifarious, multiplexed *Burkholderia cepacia* complex. *Nat. Rev. Microbiol.* 3, 144–156.
- Martin, D. W., and Mohr, C. D. (2000) Invasion and intracellular survival of *Burkholderia cepacia*. *Infect. Immun.* 68, 24–29.
- Saini, L. S., Galsworthy, S. B., John, M. A., and Valvano, M. A. (1999) Intracellular survival of *Burkholderia cepacia* complex isolates in the presence of macrophage cell activation. *Microbiology* 145, 3465–3475.
- Ortega, X. P., Cardona, S. T., Brown, A. R., Loutet, S. A., Flannagan, R. S., Campopiano, D. J., Govan, J. R., and Valvano, M. A. (2007) A putative gene cluster for aminoarabinose biosynthesis is essential for *Burkholderia cenocepacia* viability. *J. Bacteriol.* 189, 3639–3644.
- Gunn, J. S., Lim, K. B., Krueger, J., Kim, K., Guo, L., Hackett, M., and Miller, S. I. (1998) PmrA-PmrB-regulated genes necessary for 4-aminoarabinose lipid A modification and polymyxin resistance. *Mol. Microbiol.* 27, 1171–1182.
- Flannagan, R. S., Aubert, D., Kooi, C., Sokol, P. A., and Valvano, M. A. (2007) *Burkholderia cenocepacia* requires a periplasmic HtrA protease for growth under thermal and osmotic stress and for survival in vivo. *Infect. Immun.* 75, 1679–1689.
- Leduc, R. D., Taylor, G. K., Kim, Y. B., Janusz, T. E., Bynum, L. H., Sola, J. V., Garavelli, J. S., and Kelleher, N. L. (2004) ProSight PTM: an integrated environment for protein identification and characterization by top-down mass spectrometry. *Nucleic Acids Res.* 32, W340–W345.
- Leduc, R. D., and Kelleher, N. L. (2007) Using ProSight PTM and related tools for targeted protein identification and characterization with high mass accuracy tandem MS data, Current Protocols in Bioinformatics, Chapter 13, Unit 13.6.
- Lee, S. P., Hwang, Y. S., Kim, Y. J., Kwon, K. S., Kim, H. J., Kim, K., and Chae, H. Z. (2001) Cyclophilin A binds to peroxidoredoxins and activates its peroxidase activity. *J. Biol. Chem.* 276, 29826–29832.
- Monteiro, G., Horta, B. B., Pimenta, D. C., Augusto, O., and Netto, L. E. (2007) Reduction of 1-Cys peroxidoredoxins by ascorbate changes the thiol-specific antioxidant paradigm, revealing another function of vitamin C. *Proc. Natl. Acad. Sci. U.S.A.* 104, 4886–4891.
- Noguera-Mazon, V., Lemoine, J., Walker, O., Rouhier, N., Salvador, A., Jacquot, J. P., Lancelin, J. M., and Krimm, I. (2006) Glutathionylation induces the dissociation of 1-Cys D-peroxidoredoxin non-covalent homodimer. *J. Biol. Chem.* 281, 31736–31742.
- Rouhier, N., Gelhaye, E., Sautiere, P. E., Brun, A., Laurent, P., Tagu, D., Gerard, J., de, F. E., Meyer, Y., and Jacquot, J. P. (2001) Isolation and characterization of a new peroxidoredoxin from poplar sieve tubes that uses either glutaredoxin or thioredoxin as a proton donor. *Plant Physiol.* 127, 1299–1309.
- Rouhier, N., Gelhaye, E., and Jacquot, J. P. (2002) Glutaredoxin-dependent peroxidoredoxin from poplar: protein-protein interaction and catalytic mechanism. *J. Biol. Chem.* 277, 13609–13614.
- Ghrist, A. C., and Stauffer, G. V. (1995) Characterization of the *Escherichia coli* *gcvR* gene encoding a negative regulator of *gcv* expression. *J. Bacteriol.* 177, 4980–4984.
- Ghrist, A. C., and Stauffer, G. V. (1998) Promoter characterization and constitutive expression of the *Escherichia coli* *gcvR* gene. *J. Bacteriol.* 180, 1803–1807.
- Abreu-Goodger, C., Ontiveros-Palacios, N., Ciria, R., and Merino, E. (2004) Conserved regulatory motifs in bacteria: riboswitches and beyond. *Trends Genet.* 20, 475–479.
- Lamothe, J., Thyssen, S., and Valvano, M. A. (2004) *Burkholderia cepacia* complex isolates survive intracellularly without replication within acidic vacuoles of *Acanthamoeba polyphaga*. *Cell Microbiol.* 6, 1127–1138.
- Saini, L. S., Galsworthy, S. B., John, M. A., and Valvano, M. A. (1999) Intracellular survival of *Burkholderia cepacia* complex isolates in the presence of macrophage cell activation. *Microbiology* 145, 3465–3475.
- Valvano, M. A., Keith, K. E., and Cardona, S. T. (2005) Survival and persistence of opportunistic *Burkholderia* species in host cells. *Curr. Opin. Microbiol.* 8, 99–105.
- Holden, M. T., Seth-Smith, H. M., Crossman, L. C., Sebailia, M., Bentley, S. D., Cerdeno-Tarraga, A. M., Thomson, N. R., Bason, N., Quail, M. A., Sharp, S., Cherevach, I., Churcher, C., Goodhead, I., Hauser, H., Holroyd, N., Mungall, K., Scott, P., Walker, D., White, B., Rose, H., Iversen, P., Mil-Homens, D., Rocha, E. P., Fialho, A. M., Baldwin, A., Dowson, C., Barrell, B. G., Govan, J. R., Vandamme, P., Hart, C. A., Mahenthalingam, E., and Parkhill, J. (2009) The genome of *Burkholderia cenocepacia* J2315, an epidemic pathogen of cystic fibrosis patients. *J. Bacteriol.* 191, 261–277.
- Liao, S. J., Yang, C. Y., Chin, K. H., Wang, A. H., and Chou, S. H. (2009) Insights into the alkyl peroxide reduction pathway of *Xanthomonas campestris* bacterioferritin comigratory protein from the trapped intermediate-ligand complex structures. *J. Mol. Biol.* 390, 951–966.
- Wang, G., Olczak, A. A., Walton, J. P., and Maier, R. J. (2005) Contribution of the *Helicobacter pylori* thiol peroxidase bacterioferritin comigratory protein to oxidative stress resistance and host colonization. *Infect. Immun.* 73, 378–384.
- Keith, K. E., Killip, L., He, P., Moran, G. R., and Valvano, M. A. (2007) *Burkholderia cenocepacia* C5424 produces a pigment with antioxidant properties using a homogentisate intermediate. *J. Bacteriol.* 189, 9057–9065.
- Keith, K. E., and Valvano, M. A. (2007) Characterization of SodC, a periplasmic superoxide dismutase from *Burkholderia cenocepacia*. *Infect. Immun.* 75, 2451–2460.
- Lefebvre, M., and Valvano, M. (2001) In vitro resistance of *Burkholderia cepacia* complex isolates to reactive oxygen species in relation to catalase and superoxide dismutase production. *Microbiology* 147, 97–109.
- Lefebvre, M. D., Flannagan, R. S., and Valvano, M. A. (2005) A minor catalase/peroxidase from *Burkholderia cenocepacia* is required for normal aconitase activity. *Microbiology* 151, 1975–1985.
- Chung, J. W., and Speert, D. P. (2007) Proteomic identification and characterization of bacterial factors associated with *Burkholderia cenocepacia* survival in a murine host. *Microbiology* 153, 206–214.
- Lamothe, J., Huynh, K. K., Grinstein, S., and Valvano, M. A. (2007) Intracellular survival of *Burkholderia cenocepacia* in macrophages is associated with a delay in the maturation of bacteria-containing vacuoles. *Cell Microbiol.* 9, 40–53.
- Taylor, P. D., Inchley, C. J., and Gallagher, M. P. (1998) The *Salmonella typhimurium* AhpC polypeptide is not essential for virulence in BALB/c mice but is recognized as an antigen during infection. *Infect. Immun.* 66, 3208–3217.
- Mahenthalingam, E., Coenye, T., Chung, J. W., Speert, D. P., Govan, J. R., Taylor, P., and Vandamme, P. (2000) Diagnostically and experimentally useful panel of strains from the *Burkholderia cepacia* complex. *J. Clin. Microbiol.* 38, 910–913.